Polypyrrole Nanopipes as a Promising Cathode Material for Li‐ion Batteries and Li‐ion Capacitors: Two‐in‐One Approach

Dr. Deepak Dubal Dr. Ajay Jagadale Dr. Nilesh R. Chodankar Prof. Do‐Heyoung Kim Prof. Dr. Pedro Gomez‐Romero Prof. Rudolf Holze*

Dr. D. Dubal
School of Chemical Engineering, The University of Adelaide, Adelaide, South Australia 5005, Australia E-mail:dubaldeepak2@gmail.com

Dr. D. Dubal, Prof. Dr. P. Gomez-Romero
Catalan Institute of Nanoscience and Nanotechnology (ICN2), CSIC and the Barcelona Institute of Science and Technology, Campus UAB, Bellaterra 08193, Barcelona, Spain

Dr. A. Jagadale
Department of Electrical and Electronics Engineering, School of Electrical and Electronics Engineering, SASTRA Deemed University, Thanjavur 613001, Tamilnadu, India

Dr. N. R. Chodankar, Prof. D.-H. Kim
School of Applied Chemical Engineering, Chonnam National University, Gwangju500-757, South Korea

Prof. R. Holze Technische Universität Chemnitz, Institut für Chemie, AG Elektrochemie,D-09107 Chemnitz, Germany

KEYWORDS: Polypyrrole cathode,·High energy density,·Lithium ion capacitor

ABSTRACT: Lithium ion capacitor (LIC) is a promising energy storage system that can simultaneously provide high energy with high rate (high power). Generally, LIC is fabricated using capacitive cathode (activated carbon, AC) and insertion‐type anode (graphite) with Li‐ion based organic electrolyte. However, the limited specific capacities of both anode and cathode materials limit the performance of LIC, in particular energy density. In this context, we have developed “two in one” synthetic approach to engineer both cathode and anode from single precursor for high performance LIC. Firstly, we have engineered a low cost 1D polypyrrole nanopipes (PPy‐NPipes), which was utilized as cathode material and delivered a maximum specific capacity of 126 mAh/g, far higher than that of conventional AC cathodes (35 mAh/g). Later, N doped carbon nanopipes (N‐CNPipes) was derived from direct

carbonization of PPy‐NPipes and successfully applied as anode material in LIC. Thus, a full LIC was fabricated using both pseudo‐capacitive cathode (PPy‐NPipes) and anode (N‐CNPipes) materials, respectively. The cell delivered a remarkable specific energy of 107 Wh/kg with maximum specific power of 10 kW/kg and good capacity retention of 93 % over 2000 cycles. Thus, this work provide a new approach of utilization of nanostructured conducting polymers as a promising pseudocapacitive cathode for high performance energy storage systems.

1 Introduction

High energy and power densities along with longer cycle life are the main requirements of the current energy storage technology. Due to the fast progress in electronic devices, electrical vehicles and large scale grid energy storage, high performance energy storage devices very much needed.[1] Supercapacitors (SCs) and lithium ion batteries (LIBs) have attracted great attention because of their wide range of applications in our daily life.[2] LIBs are well-known for high energy density (around 150–200 Wh/kg), however batteries exhibit poor power as well as cyclic stability. Conversely, SCs show high power density (2–5 kW/kg) and excellent cycling stability devices but suffer of low energy density.[3] Therefore, it is desirable to combine the advances of both LIBs and SCs in a single device to develop high performance hybrid energy storage devices.

Lithium ion capacitor (LIC) is an advanced energy storage device which has the ability to bridge the gap between LIBs and SCs. Basically, LICs are made up of capacitive-type cathode materials, battery-type anode material, and lithium salt in the organic solvent-based electrolyte solution with wide working potential window.[4,5] Currently, there have been many challenges to fabricate high performance LICs with both high energy and power density. The poor specific capacity (30–35 mAh/g) of commonly utilized AC cathodes conciliates the large

capacity of the battery-type anode, which leads to low energy density of LIC. Anodes with different storage mechanisms such as the insertion-type, conversion-type and alloy-type one have been used. For instance, anodes such as graphite6 and $Li_4Ti_5O_{12}$ (LTO)[7] belong to the insertion-type family, which have acceptable cyclic stabilities but their limited specific capacities deteriorate the energy density of the LIC. In addition, Fe_2O_3 and MnO (conversion-type anodes) as well as Si and Sn (alloy-type anodes) can deliver good specific capacities but suffer of poor cyclic stability as well as rate capability. As far as cathodes are concerned, they possess ECDL-type charge storage mechanism in which charges are accumulated on the surface at the interface between electrode and electrolyte. Here, charges are stored physically on the electrode surface which results in poor specific capacitance as well as specific capacity. The specific capacity of the cathode can be improved by enhancing the specific surface area and the electrochemical activity by doping heteroatoms which not only increases the capacitance but also the rate capability of the electrode. Recently, various strategies have been used in order to improve the specific capacity of the cathode.[8-11] For example, Wang et al.[12] have prepared ZIF-8105 derived a porous carbon cathode via carbonization which delivered the maximum specific capacity of 105.1 mAh/g at 1A/g. In another study, Won et al.[13] have synthesized N-rich carbon nanotubes for LIC application which showa specific capacity of 74.6 mAh/g at a current density of 200 mA/g. Owing to the fast surface redox reactions at the electrode/electrolyte interface, the pseudo-capacitive cathode materials can enhance the performance of LIC than that by conventional AC cathode.[14,15] Among these materials, conducting polymers have attracted great attention because of their low cost, high specific capacitance and facile synthesis. Polypyrrole is one of the best pseudocapacitive materials frequently reported in the literature.[16-20] As per our knowledge, there is no report on utilizing polypyrrole (PPy) as a cathode in LIC.

In the present work, we have engineered one-dimensional (1D) hollow polypyrrole nanopipes (PPy-NPipes) as a cathode material for Li-ion battery. Later, PPy-NPipes were employed as a precursor to prepare nitrogen-doped carbon nanopipes (N-CNPipes). Prior to fabrication of LICs, the performance of PPy-NPipes and N-CNPipes were investigated in a half-cell configuration. The full LIC was subsequently assembled using PPy-NPipes as a cathode and N-CNPipes as anode materials in lithium salt containing organic electrolyte. Thus, two main strategies have been developed in this work: 1) use of conducting polymer (PPy) as cathode in LIBs and 2) two-in-one precursor approach in order to develop high performance LIC for various applications.

2 Experimental

2.1 Synthesis of PPy‐NPipes and N‐CNpipes

In a typical synthesis, 5 mM MO (sodium 4-[40 (dimethylamino)phenyldiazo] phenylsulfonate ($(CH_3)_2NC_6H_4{-}N{=}NC_6H_4SO_3Na$) and 1.5 mM $FeCl_3$ (0.243g) were dissolved in 30 ml double distilled water (DDW) which yielded a flocculent precipitate. Afterwards, 0.1 ml (1.5 mM) pyrrole monomer was added to above solution and the mixture was stirred at room temperature for 24 h. Later on, the formed precipitate was filtered and thoroughly washed with a mixture of DDW and ethanol to get neutral pH. Finally, the filtered product was dried for 12 h under vacuum at 80 °C to obtain PPy‐NPipes powder. Furthermore, N doped carbon nanopipes (N‐CNTs) were prepared by carbonizing the synthesized PPy‐NPipes at 800 °C for 1 h with a heating rate of 5 °C min−1 under N_2 atmosphere.

2.2 Material characterization

The surface morphology of PPy‐NPipes and N‐CNpipes samples was examined using a field‐emission scanning electron microscopy, FE‐SEM (FEI Quanta 650F Environmental

SEM) and transmission electron microscopy, TEM (Tecnai G2 F20 S‐TWIN HR(S) TEM, FEI). The energy‐dispersive X‐ray spectroscopy (EDS) analyzer was attached to the FE‐SEM which was used to figure out the elemental composition. The electronic states of the various elements in the sample were observed using X‐ray photoelectron spectroscopy (XPS, SPECS Germany, PHOIBOS 150). Thermogravimetric analysis of sample was carried out using Pyris 1 TGA Perkin Elmer.

2.3 Electrochemical characterization

Both electrodes were prepared by mixing the active material (PPy‐NPipes or N‐CNpipes), Super‐P conductive carbon black (Alfa Aesar 99.9 % with specific surface area of 62 m^2/g) and polyvinylidene fluoride binder (PVDF) in N‐methyl‐2‐pyrrolidone (NMP) at a 85 % :10 % :5 % ratio. The obtained slurry was uniformly coated onto Al or Cu foil, dried at 100 °C for 12 h, and pressed via hydraulic press. Cyclic voltammetry (CV) and galvanostatic charge/discharge (GCD) were carried out on a Biologic SP‐300 potentiostat. Initially, the PPy‐NPipes and N‐CNpipes were tested in half‐cell configuration using Swagelok‐type cells in an Ar‐filled glove box with lithium metal as both counter and reference electrodes. Glass fiber and 1 M lithium hexafluorophosphate in a 1:1 mixture of ethylene carbonate and dimethyl carbonate (1:1, EC: DMC) were used as a separator and electrolyte, respectively. The PPy‐NPipes were tested between 1.5V to 4.5V (vs Li/Li^+) and that of N‐CNPipes between 0.01V to 3V (vs Li/Li^+), respectively. The mass loading of PPy‐NPipes and N‐CNPipes was estimated to be 0.8 mg/cm2 and 1.1mg/cm2, respectively. Before the fabrication of full LIC, N‐CNpipes was prelithiated (discharged to 0.01V) by cycling the half‐cell at 0.5A/g. Full cell was fabricated and tested within 0.01–4V. The total mass loading of both

electrodes in full N‐CNPipes//PPy‐NPipes was maintained at 4 mg/cm2. Different electrochemical parameters were evaluated using the following formulae,

$$C\left(\frac{F}{g}\right)=\frac{I(A)\times t(s)}{t(s)3600\times m(g)}=\frac{mAh}{g}x\frac{3600}{dV(mV)} \quad (1)$$

where, 'C' is specific capacitance, 'I' is the applied current, 't' is the discharge time, m is the weight of the active material and dV is the testing potential window of the single electrode configuration (mV). The energy density (E) and power density (P) of the Li‐ion hybrid capacitor were calculated using following equations, respectively.

$$P=\frac{\Delta V\ x\ i}{m} P=\Delta V\times im \quad (2)$$

$$E=\frac{P\ x\ t}{3600} \quad (3)$$

$$\Delta V=\frac{E_{max}-E_{min}}{2} \quad (4)$$

3 Results and Discussion

As shown in **Figure 1**, PPy‐NPipes were prepared via a chemical oxidation mediated soft template‐directed route using anions azo dye methyl orange (MO). The detailed growth mechanism of PPy‐NPipes is explained elsewhere.[21-23] Further, N‐CNpipes were obtained via carbonization of PPy‐NPipes at 800 °C for 1 h with a heating rate of 5 °C min^{-1} under N_2 atmosphere (see **Figure S1** for TGA analysis). Corresponding TEM images depict no significant change in the structure of PPy‐NPipes after carbonization and show similar hollow pipe‐like structure. To study the structural properties of the prepared material, Raman, XPS and TEM analysis was carried out. Raman spectroscopy was employed in order to provide structural fingerprints of the samples. **Figure 2 (a)** shows the Raman spectra of

PPy‐NPipes and N‐CNpipes samples. Two major peaks at 1564 and 1360 cm^{-1} were observed for the spectrum of PPy‐NPipes which might be attributed to the C−C stretching vibrations in the pyrrole ring and C−H, N−H in‐plane bending vibrations.[24] On the other hand, the spectrum of N‐CNpipes showed bands at 1576 and 1357 cm^{-1} which are ascribed to the graphitic G‐ and D‐bands. Graphitic band is denoted for the C=C stretching vibration of any pair of sp2 sites and D‐band is associated with the breathing of aromatic rings which are supposed to be activated due to the defects induced by N‐doping.[25] Furthermore, to identify elements and oxidation states of both PPy‐NPipes and N‐CNpipes samples, XPS was carried out. the corresponding results are given in **Figure 2b**. The wide range XPS spectra of PPy‐NPipes and N‐CNpipes (**Figure S2** (a)), highlight the existence of C1s, N1s and O1s peaks. It is seen that the intensities of N1s and O1s peaks are reduced with the increase of C1s peak intensity in N‐CNpipes spectrum which confirms the successful carbonization of the sample. **Figure 2b** shows the N1s high resolution spectra for the PPy‐NPipes and N‐CNPipes. PPy‐NPipes exhibit two Gaussian peaks centered at 399.7 and 401.2eV that are associated with benzenoid amine (−N^{+}H−) and protonated benzenoid amine (−NH−), respectively.[26,27] After carbonization, the N1s spectrum of N‐CNPipes changes significantly with peaks now centered at 398.1 and 400.5 e, They can be identified as pyrrolic nitrogen and hexagonal pyridinic nitrogen, respectively.[28] The peak at 398.2 eV is attributed to the p‐conjugated system with a pair of p‐electrons whereas the peak at 400.9eV is observed only when the carbon atoms are substituted by nitrogen to form the ‘graphitic’ nitrogen. From these results, it is clear that both PPy‐NPipes and N‐CNpipes were formed with nitrogen of different oxidation states enabling the production of nitrogen doped N‐CNpipes. The amount of nitrogen in N‐CNPipes was calculated by the ratio of the area of the N peak and the sum of C and N peaks (N/(C+N)), and was determined

to be 12.8 % (see table in **Figure S2**). High‐resolution spectra of C1s are shown in the Figure S2 (b). In the C1s spectrum of PPy‐NPipes, the peak centered at (285.0 eV) lowest energy can be attributed to β‐carbons in the pyrrole ring whereas the peak centered at 285.0eV ascribed to α‐carbons in the ring. The third broad peak centered at 286.3eV is due to the overlap of C=N, carbonyl groups, or carbon bonded to oxygen.[29] Furthermore, the C1s peak for N‐CNpipes is presented in the same figure. These data are fitted with three peaks which are centered at 284.7 (C−C), 285.6 (C−N) and 287.7eV (C=O). This suggests that the PPy‐NPipes exhibit the presence of oxygen and nitrogen.[30]

Figure 2 (c, d) show TEM images of PPy‐NPipes and N‐CNpipes, respectively. The PPy‐NPipes are well separated from each other without aggregation. The length of PPy‐NPipes is several micrometers with diameters about 50nm. Such an open porous and nanoscaled tubular structure is promising for electrochemical charge storage application (**Figure S3**). It seems that the microstructure of the PPy‐NPipes sample doesn't change significantly after carbonization as seen in **Figure 2d**. It is worth noting that even at the high carbonization temperature of 800 °C the 1D structure of PPy‐NPipes remains unchanged. The energy‐filtered TEM (EFTEM) elemental mapping of carbon and nitrogen in N‐CNPipes is shown in **Figure 2f**. It is clearly seen that carbon and nitrogen are uniformly distributed over the nanotubular structure. This uniformly doped nitrogen facilitates homogeneously active electrochemical sites for redox reactions during charging‐discharging processes. Previously, Li et al.[31] have prepared similar microstructure of MnO@carbon nanopipes via ultrasonication and calcination treatments for energy storage application. Ramana et al.[32] have synthesized a composite of carbon nanopipes and polyaniline nanofibers via in situ chemical oxidative polymerization for the same application. Nitrogen adsorption/desorption isotherm for PPy‐NPipes and N‐CNPipes were further measured and

shown in **Figure S4**. The BET surface area was found to be 68 and 89 m^2/g for PPy‐NPipes and N‐CNPipes, respectively with mesoporous nature, suggesting porous network of nanopipes.

3.1 The cathode: Polypyrrole nanopipes (PPy‐NPipes)

In order to understand the charge storage kinetics in the PPy‐NPipes, the capacitive (outer) and diffusion controlled (inner) contributions to the total charge storage were evaluated according to the methods reported in the literature.[33] The cyclic voltammograms (CVs) at various scan rates from 1 to 10mV s^{-1} are shown in **Figure 3a**. These CV curves display weak redox peaks for PPy‐NPipes cathode, suggesting that the capacitance results from pseudocapacitive behavior. It is possible to determine the storage mechanism by examining the dependence of the current i on the scan rate v.[33]

$$i = av^b b \tag{5}$$

wherein ‘a’ and ‘b’ are adjustable parameters., At b=0.5 charge storage is associated with a semi‐infinite diffusion process while for b=1, the charge storage corresponds to a capacitive process. The value of b is the slope of the plot of log (i in mA) versus log (scan rate in mV/s). We have calculated b‐values at different potentials; results are presented in **Figure 3b**. It is revealed that b‐values lies in between 0.8 to 0.95 for potentials in the range of 2.5–4.0 V (vs Li/Li^+), which clearly confirms that the charge contribution mainly comes from capacitive reactions (EDLC and pseudo‐capacitive). It is necessary to investigate the storage contributions of cathode materials in order to find out the better capacitive cathode for LIC

fabrication. The total charge storage (q_t) is the sum of surface controlled (q_c) and diffusion controlled (q_d) charge storage as presented below,

$$q_t = q_c + q_d \quad (6)$$

The capacitive contribution (q_c) is scan rate dependent because the charge storage results from the accumulation of charges as well as fast surface redox reactions. Therefore, it is supposed to be a combination of both EDLC and pseudocapacitive type charge storage. On the other hand, diffusion controlled (q_d) contribution is due to the diffusion processes in the electrode which change with the reciprocal of square root of scan rate. Hence the total charge contribution can be written as,

$$q_t = q_c + kv^{1/2} \quad (7)$$

wherein k is a constant and qc can be evaluated from the plot of q_t versus the reciprocal of the square root of the scan rate ($v^{-1/2}$). **Figure 3c** shows the capacitive charge storage contributions of PPy‐NPipes at the scan rates from 1 to 10 mV/s. At the scan rate of 1 mV/s the capacitive contribution is around 60 % and the remaining 40 % are due to the diffusion controlled contribution. Excellent capacitive contribution at a low scan rate of 1 mV/s is ascribed to the fast redox reactions and good electronic conductivitye of the PPy‐NPipes. At higher scan rates, the capacitive contribution reaches up to 80 %. In LIC, it is desirable to have a cathode with high surface charge storage contribution which helps to improve the rate capability of the device. The appreciable surface contribution in the present case is attributed to the nanopipe‐like structure of the PPy material which facilitates high surface area as well as open channels for electrolyte diffusion. The good conductivity and interconnections

between PPy‐NPipes help to advance the electronic diffusion through the electrode network.[34] **Figure 3d** shows galvanostatic charge‐discharge (GCD) curves of PPy‐NPipes recorded at different current densities from 0.14A/g to 13.8A/g. It is seen that the curves are non‐linear which indicates the pseudocapacitive type of storage mechanism in PPy‐NPipes. Interestingly, the PPy‐NPipes cathode shows a maximum capacity of 126mA/g at 0.14A/g, which is far greater than that of activated carbon or other carbonaceous cathodes.[8,9,12] It is worth mentioning that even at the higher current density of 13.8A/g, the PPy‐NPipes cathode still offers a capacity of 50mAh/g, indicating good rate performance (Figure 3e). Interestingly, when number of cycles increased, capacities calculated at each current density do not change significantly even at the higher current density suggesting excellent cyclic stability of the cathode. After 80 cycles capacities calculated at the current density of 0.34A/g achieve similar values without significant loss. The cyclic stability of the PPy‐NPipe cathode was tested at current density of 0.34A/g for 500 cycles. Impressively, there is no significant loss in the capacity of PPy nanopipes over 500 cycles. The Coulombic efficiency of the PPy‐NPipes cathode is maintained at 100 %. Due to the pseudocapacitive nature of the electrode, cyclic stability was found to be acceptable since it is a molecular redox process with no phase transition and volume change during charging‐discharging. The results are excellent when compared to previous investigations on PPy‐based cathode materials.35 For instance, Qie et al.[35] prepared PPy nanoparticles using different dopants and reported a maximum capacity of 122mAh/g at 7.2mA/g with 89.9 % capacity retention after 600 cycles. Such a high capacity and excellent cycling stability might correspond to hollow tubular nanostructures of PPy where the ultra‐long nanopipes serve as channels for electron transportation as well as act as reservoirs for storage of Li+‐ions. In addition, huge inner space (around 40 nm) and very thin walls (15–17 nm) provide extra‐space and short

diffusion paths for Li‐ion as well as offer sufficient electrode/electrolyte interface to absorb Li^+‐ions and promote rapid charge‐transfer reaction.

3.2 Full cell: N‐CNPipes//PPy‐NPipes Li‐Ion capacitor (LIC)

For a full LIC we have prepared N‐CNPipes by direct carbonization of PPy‐NPipes and utilized them as anode material in a Li‐ion battery. The electrochemical performance of N‐CNPipes as anode in a half‐cell configuration is shown in **Figure 4 (a)**. The CV curves recorded at a scan rate of 1mV s−1 for N‐CNpipes exhibits similar trend as the carbon based anodes.[36] To determine the charge storage kinetics the b‐values at different potentials were estimated using equation (1); results are shown in **Figure 4 (b)**. It is interesting to note that the b‐values are between 0.72 and 0.82, suggesting that surface capacitive storage dominates the diffusion‐controlled process. The shaded CV in **Figure 4 (a)** corresponds to the capacitive contribution of the N‐CNPipes, which is found to be 56 % at 1 mV/s. In addition, we have calculated the capacitive charge contribution at different scan rates, results are presented in **Figure 4 (c)**. It is seen that the capacitive contribution increases with scan rate (**Figure S5**).

The first three galvanostatic charge/discharge (GCD) curves for N‐CNPipes at the current density of 0.2 A/g are shown in **Figure 4** (d). It is seen that the potential falls rapidly during first discharge and forms a plateau at 0.9–0.7V, which might correspond to the SEI layer formation.[25] The initial reversible capacity was obtained as 815mAh/g, which was stabilized to 652mAh/g after a few charge/discharge cycles. The present value of reversible capacity is quite comparable to the recently reported capacities for carbon‐based anodes.[37,38,39] In

addition, the N‐CNPipes electrode exhibited good cycling stability over 500 cycles measured at 0.1A/g (**Figure S6**).

Thus, N‐CNPipes and PPy‐NPipes were successfully implemented as anode and cathode materials with average working potentials of 0.7V and 3.5V (vs Li/Li^+) in Li‐ion batteries. These preliminary results confirm the suitability of these materials in LIC. **Figure 5 (a)** shows CV curves for both N‐CNPipes and PPy‐NPipes electrodes within potential windows of 0.01–3V and 1.5–4.5V (vs. Li/Li^+), respectively. This complementary potential windows will lead to a wide operating voltage for full LIC devices. Before the fabrication of the LICs, both PPy‐NPipes and N‐CNPipes electrodes were pre‐activated for 10 cycles at 0.25A/g in Li‐half cells. N‐CNPipes anode was fully charged via lithiation up to 0.01V (vs Li) in order to achieve best performance of full LIC cell. Before assembling the LIC cell, the charges on both the electrode was balanced to achieve the best electrochemical performance. The charges on both electrode was maintained by calculating the mass ratio from N‐CNPipes to PPy‐NPipes (5.1:1). Figure5 (b) with the inset shows the GCD curves for N‐CNPipes//PPy‐NPipes LIC at various current densities ranging from 0.17 to 6.67A/g within the potential window of 0.01 to 4.5V. As expected, the GCD curves are nonlinear in nature, which is attributed to the pseudocapacitive mechanism of both electrodes. Further, this GCD data was employed to calculate specific capacity and capacitance of the LIC cell using formulae listed in the experimental section. **Figure 5 (c)** shows the variation of specific capacity and capacitance with different current densities. The capacitance/capacity decreased with growing current density, which might be attributed to the fact that at high current rates, only outer surfaces of the electrodes are involved in the electrochemical reaction that leads to the lower values of both capacity and capacitance. Besides, at the lower current density of 0.17A/g, a maximum specific capacity and capacitance were reported as 80mAh/g and 85F/g,

respectively. Furthermore, the energy and power densities of the LIC were calculated and plotted as a Ragone plot in the **Figure 5 (d)**. It shows the energy and power densities of N‐CNPipes//PPy‐NPipes LIC at various current densities and their comparison with values reported in the literature.[40-47] Our present N‐CNPipes//PPy‐NPipes LIC device shows the maximum specific energy of 107Wh/kg at specific power of 250W/kg. Nevertheless, at maximum specific power 10000W/kg, LIC can still deliver the specific energy of 49Wh/kg. It is worth mentioning that the current values are quite comparable with the values reported in the literature.[40-47] Furthermore, the cyclic stability of the N‐CNPipes//PPy‐NPipes LIC was examined at current density of 1A/g for 2000 cycles as shown in **Figure 5 (e).** The specific capacity of LIC initially increased during the first 110 cycles and then stabilized around 100 %, which might correspond to the surface activation of electrodes.[48,49] An excellent stability was found with the capacity retention of 93 % after 2000 cycles with very stable Coulombic efficiency of 100 %.

This significant performance of N‐CNPipes//PPy‐NPipes in the present case can be credited to the following reasons. i) both N‐CNPipe and PPy‐NPipe electrodes exhibit unique open porous and ultra‐long tubular nanostructure, which facilitates fast ionic and electronic transport through the electrode network. ii) Interestingly, both N‐CNPipes and PPy‐NPipes exhibit pseudo‐capacitive charge storing mechanism, which offers rapid charge/discharge reactions with good energy densities. iii) N‐doping in N‐CNPipes can improve the electrochemical reactivity and electronic conductivity.

4 Conclusions

In summary, we have successfully fabricated a high energy, stable LIC using single precursor formulated N‐CNPipes and PPy‐NPipes as anode and cathode, providing a cost effective "two‐in‐one" synthetic approach. Both electrodes showed good reversible capacity as anode (N‐CNPipes) and cathode (PPy‐NPipes) in Li‐ion half‐cell configuration. It should be emphasized that both electrodes store charges through fast and highly reversible pseudo‐capacitive mechanism. A full LIC cell with pseudo‐capacitive cathode (PPy‐NPipes) and anode (N‐CNPipes) delivered a remarkable specific energy of 107 Wh/kg with maximum specific power of 10 kW/kg and good capacity retention of 93 % over 2000 cycles. Thus, this work provides a new approach to utilization of nanostructured conducting polymers as a promising pseudocapacitive cathode as well as a cost effective "two‐in‐one" synthetic strategy to develop low cost materials for high performance energy storage systems.

Acknowledgements

DPD acknowledges support of University of Adelaide, Australia by University Research Fellowship (Research for Impact Fellow). The ICN2 is supported by the Severo Ochoa program of the Spanish Ministry of Economy, Industry, and Competitiveness (MINECO, grant no. SEV‐2013‐0295) and funded by the CERCA program/Generalitat de Catalunya.

References

[1] a) D. P. Dubal,O. Ayyad,V. Ruiz, P. Gomez-Romero, Chem. Soc. Rev. **2015**, 44, 1777–1790.b) X. Luo, J. Wang, M. Dooner, J. Clarke, Appl.Energy **2015**, 137, 511–536.
[2] L. Wang, Y. Han, X. Feng, J. Zhou, P. Qi, B. Wang, Coord. Chem. Rev. **2016**, 307, 361–381.
[3] K. A. Owusu, L. Qu, J. Li, Z. Wang, K. Zhao, C. Yang, K. M. Hercule, C. Lin, C. Shi, Q. Wei, Nat.Commun. **2017**, 8, 14264.
[4] a) D. P. Dubal, K. Jayaramulu, R. Zboril, R. A. Fischer, P. Gomez-Romero, J. Mater. Chem. A **2018**, 6, 6096–6106.b) H. Wang, C. Guan, X. Wang, H. J. Fan, Small **2015**, 11, 1470–1477.
[5] J. Luo, W. Zhang, H. Yuan, C. Jin, L. Zhang, H. Huang, C. Liang, Y. Xia, J. Zhang, Y. Gan, ACSNano **2017**, 11, 2459–2469.
[6] S. Kumagai, T. Ishikawa, N. Sawa, J. Energy Storage **2015**, 2, 1–7.
[7] L. Ye, Q. Liang, Y. Lei, X. Yu, C. Han, W. Shen, Z.-H. Huang, F. Kang, Q.-H. Yang, J. Power Sources **2015**, 282, 174–178.
[8] M. Xinlong, G. Daowei, ChemSusChem **2018**, 11, 1048–1055.
[9] B. Li, H. Zhang, D. Wang, H. Lv, C. Zhang, RSCAdv. **2017**, 7, 37923–37928.
[10] C. h. Lee, C. Jung, Electrochim. Acta **2017**, 232, 596–600.
[11] A. Jain, S. Jayaraman, M. Ulaganathan, R. Balasubramanian, V.Aravindan, M. P. Srinivasan, S. Madhavi, Electrochim. Acta **2017**, 228, 131–138.
[12] R. Wang, D. Jin, Y. Zhang, S. Wang, J. Lang, X. Yan, L. Zhang, J. Mater. Chem.A **2017**, 5, 292–302.
[13] J. H. Won, H. M. Jeong, J. K. Kang, Adv. Energy Mater. **2017**, 7, 1601355.
[14] R. Ramya, R. Sivasubramanian, M. V. Sangaranarayanan, Electrochim. Acta **2013**, 101, 109–129.
[15] C. D. Lokhande, D. P. Dubal, O.-S. Joo, Curr. Appl. Phys. **2011**, 11, 255–270.
[16] P. Asen, S. Shahrokhian, J. Phys. Chem.C **2017**, 121, 6508–6519.
[17] Y. Chen, W. Ma, K. Cai, X. Yang, C. Huang, Electrochim. Acta **2017**, 246, 615–624.
[18] H. Moon, H. Lee, J. Kwon, Y. D. Suh, D. K. Kim, I. Ha, J. Yeo, S. Hong, S. H. Ko, Sci. Rep. **2017**, 7, 41981.
[19] A. Moyseowicz, A.Śliwak, E. Miniach, G. Gryglewicz, Compos. Part B: Engineering **2017**, 109, 23–29.
[20] N. Wang, P. Zhao, K. Liang, M. Yao, Y. Yang, W. Hu, Chem. Eng. J. **2017**, 307, 105–112.
[21] X. Yang, Z. Zhu, T. Dai, Y. Lu, Macromol. Rapid Commun. **2005**, 26, 1736–1740.
[22] D. P. Dubal, N. R. Chodankar, Z. Caban-Huertas, F. Wolfart, M.Vidotti, R. Holze, C. D. Lokhande, P. Gomez-Romero, J. Power Sources **2016**, 308, 158–165.
[23] J. Kopecká, M. Mrlík, R. Olejník, D. Kopecký, M. Vrnata, J. Prokeš, P. Bober, Z. Morávková, M. Trchová, J. Stejskal, Sensors **2016**, 16, 1917.

[24] E. Alekseeva, P. Bober, M. Trchová, I. Šeděnková, J. Prokeš, J.Stejskal, Synth. Met. **2015**, 209, 105–111.
[25] D. P. Dubal, P. Gomez-Romero, Mater.Today Energy **2018**, 8, 109–117.
[26] J. Wang, Y. Xu, J. Zhu, P. Ren, J. Power Sources **2012**, 208, 138–143.
[27] M. Zhu, Y. Huang, Q. Deng, J. Zhou, Z. Pei, Q. Xue, Y. Huang, Z.Wang, H. Li, Q. Huang, Adv. Energy Mater. **2016**, 6, 1600969.
[28] L. Qie, W. M. Chen, Z. H. Wang, Q. G. Shao, X. Li, L. X. Yuan, X. L.Hu, W. X. Zhang, Y. H. Huang, Adv.Mater. **2012**, 24, 2047–2050.
[29] J. Zhou, E. R. Fisher, J. Nanosci. Nanotechnol. **2004**, 4, 539–547.
[30] Y.-N. Sun, Z.-Y. Sui, X. Li, P.-W. Xiao, Z.-X. Wei, B.-H. Han, ACS Appl. Nano Mater. **2018**, 1, 609–616.
[31] L. Li, J. Zhu, Y. Niu, Z. Chen, Y. Liu, S. Liu, M. Xu, C. M. Li, J. Jiang, ACS Sustainable Chem. Eng. **2017**, 5, 6288–6296.
[32] G. V. Ramana, P. S. Kumar, V. V. Srikanth, B. Padya, P. Jain, J. Nanosci. Nanotechnol. **2015**, 15, 1338–1343.
[33] a) W. Huanwen, Z. Yu, A. Huixiang, Z. Yongqi, T. H. Teng, Z. Yufei, G. Yuanyuan, F. J. B., W. X. Long, S. Madhavi, F. H. Jin, Y. Qingyu, Adv. Funct. Mater. **2016**, 26, 3082–3093.b) S. Ardizzone, G.Fregonara, S. Trasatti, Electrochim. Acta **1990**, 35, 263–267.
[34] D. P. Dubal, B. Ballesteros, A. A. Mohite, P. Gomez-Romero, ChemSusChem, **2017**, 10, 731–737.
[35] a) L. Qie, L. X. Yuan, W. X. Zhang, W. M. Chen, Y. H. Huang, J. Electrochem. Soc. **2012**, 159, A1624–A1629. b) G. X. Wang, L. Yang, Y. Chen, J. Z. Wang, S. Bewlay, H. K. Liu, Electrochim. Acta **2005**, 50, 4649–4654.
[36] J. Zhang, Z. Shi, J. Wang, J. Shi, J. Electroanal. Chem. **2015**, 747, 20–28.
[37] X. Zhang, G. Zhu, M. Wang, J. Li, T. Lu, L. Pan, Carbon **2017**, 116,686–694.
[38] X. Qiuying, Y. Hai, W. Min, Y. Mei, G. Qiubo, W. Liming, X. Hui, Y. Yan, Adv. Energy Mater. **2017**, 7, 1701336.
[39] Z. Cabán-Huertas, D. P. Dubal, O. Ayyad, P. Gómez-Romero, Journal of Electrochem. Sci. **2017**, 164, A6140–A6146.
[40] H. Wang, Y. Zhang, H. Ang, Y. Zhang, H. T. Tan, Y. Zhang, Y. Guo, J. B. Franklin, X. L. Wu, M. Srinivasan, H. J. Fan, Q. Yan, Adv. Funct. Mater. **2016**, 26, 3082–3093.
[41] H. Wang, C. Guan, X. Wang, H. J. Fan, Small **2015**, 11, 1470.
[42] R. Yi, S. Chen, J. Song, M. L. Gordin, A. Manivannan, D. Wang, Adv. Funct. Mater. **2014**, 24, 7433.
[43] K. Leng, F. Zhang, L. Zhang, T. Zhang, Y. Wu, Y. Lu, Y. Huang, Y.Chen, NanoRes. **2013**, 6, 581.
[44] K. Karthikeyan, S. Amaresh, S. N. Lee, V. Aravindan, Y. S. Lee, Chem. Asian J. **2014**, 9, 852.
[45] F. Zhang, T. Zhang, X. Yang, L. Zhang, K. Leng, Y. Huang, Y. Chen, Energy Environ. Sci. **2013**, 6, 1623.
[46] E. Lim, C. Jo, H. Kim, M. H. Kim, Y. Mun, J. Chun, Y. Ye, J. Hwang, K. S. Ha, K. C. Roh, K. Kang, S. Yoon, J. Lee, ACS Nano **2015**, 9, 7497.
[47] X. Wang, P. S. Lee, J. Mater. Chem. A **2015**, 3, 21706.

[48] R. Rakhi, W. Chen, D. Cha, H. Alshareef, Nano Lett. **2012**, 12, 2559.
[49] N. R. Chodankar, D. P. Dubal, Y. Kwon,Do-Heyoung Kim, NPG Asia Mater. **2017** ,9, e419.

Figure Captions

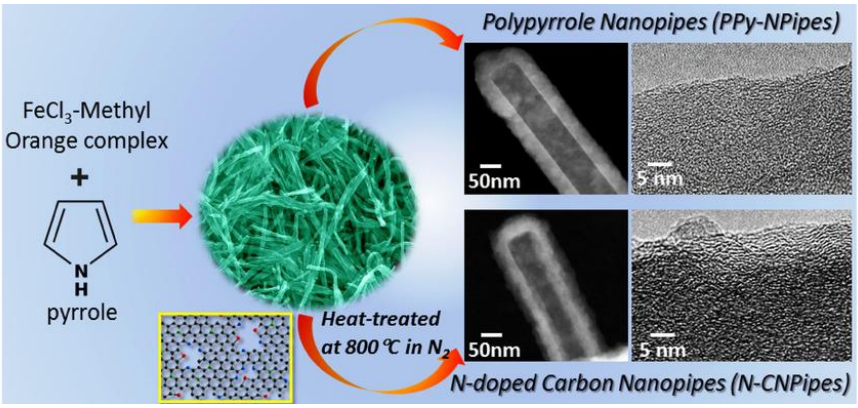

Figure 1. schematic to prepare the polypyrrole nanopipes and N‐doped carbon nanopipes from the single precursor to assemble the LICs..

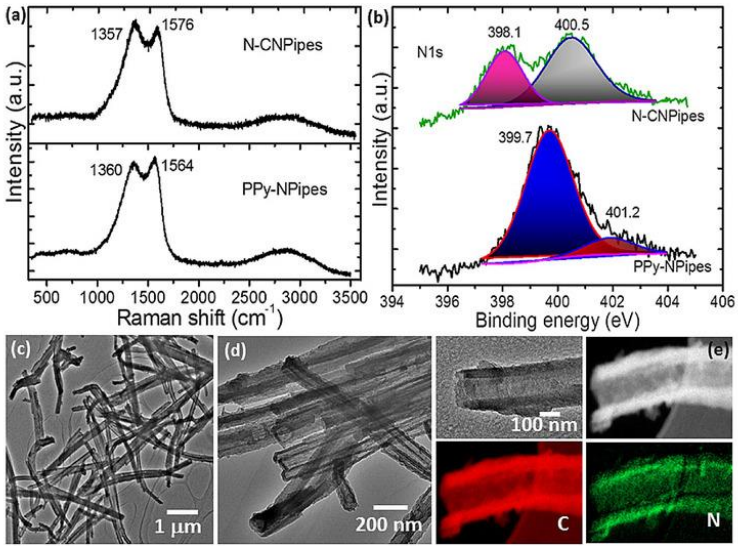

Figure 1. a) Raman and (b) N1s narrow scan XPS spectra for the PPy-NPipes and N-CNPipes. TEM images for (c) PPy-NPipes and (d) N-CNPipes, respectively. (e, f) corresponding elemental mapping for the N-CNPipes sample.

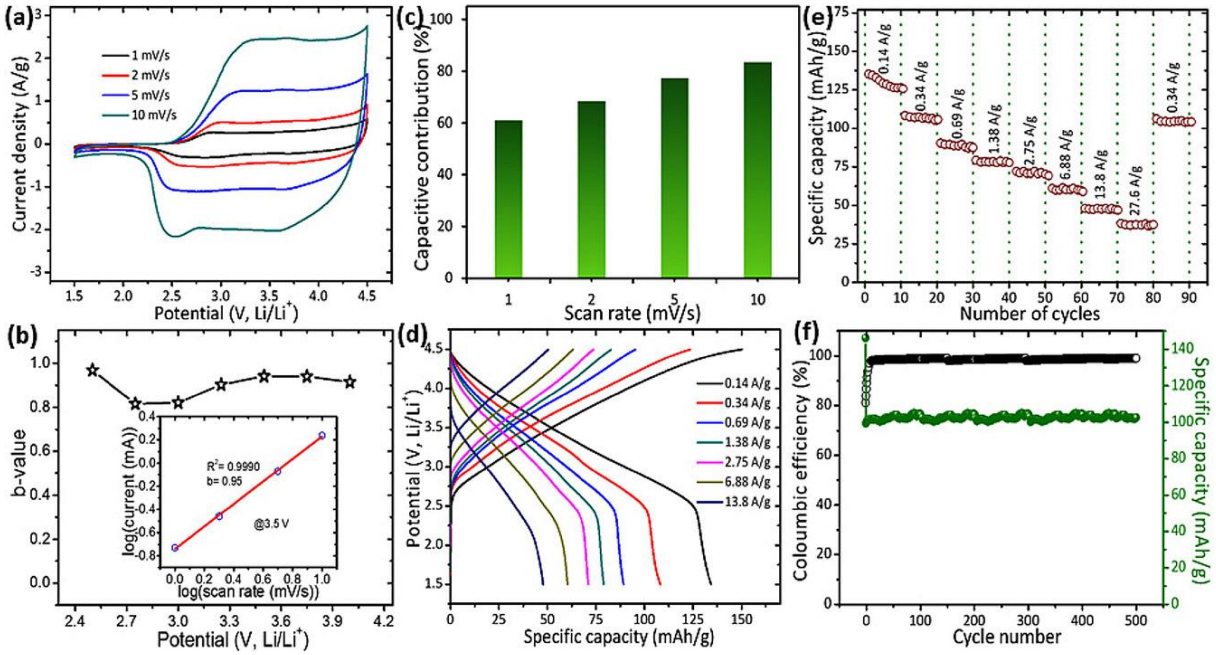

Figure 3 Electrochemical performances of PPy‐NPipes cathode in half‐cell configuration: (a) CV curves recorded at different scan rates. (b) Plot of b‐value versus potential, inset shows the log (i) versus log (scan rate). (c) Variation of capacitive charge contribution at different scan rates. (d) galvanostatic charge‐discharge (GCD) curves at different current densities from 0.14A/g to 13.8A/g, (e) Rate perforance at different current density with number of cycles and (f) variation of specific capacity and coulombic efficiency with cycle number at constant current density of 0.34A/g.

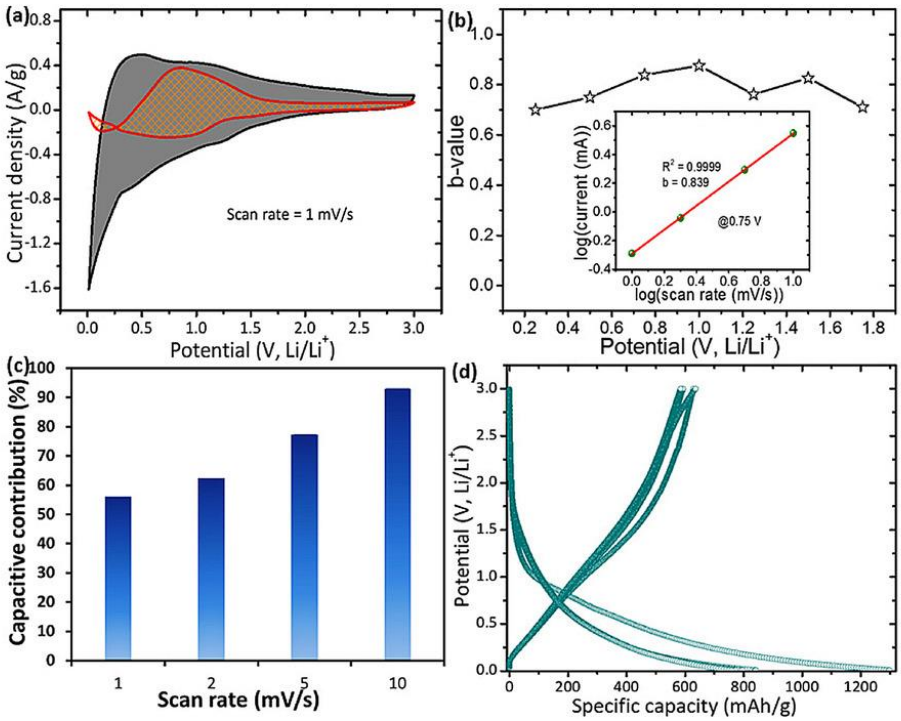

Figure 4 Electrochemical properties of N‐CNPipes anode in half‐cell configuration: (a) CV curves at the scan rate of 1 mV/s with capacitive (shaded region) and diffusion‐controlled (gray filled) contributions. (b) Plot of b‐value versus potential calculated from the slope of graph of log (i) versus log (scan rate). (c) Plot of capacitive charge contribution at different scan rates. (d) GCD curves recorded at the current density of 0.1 A/g.

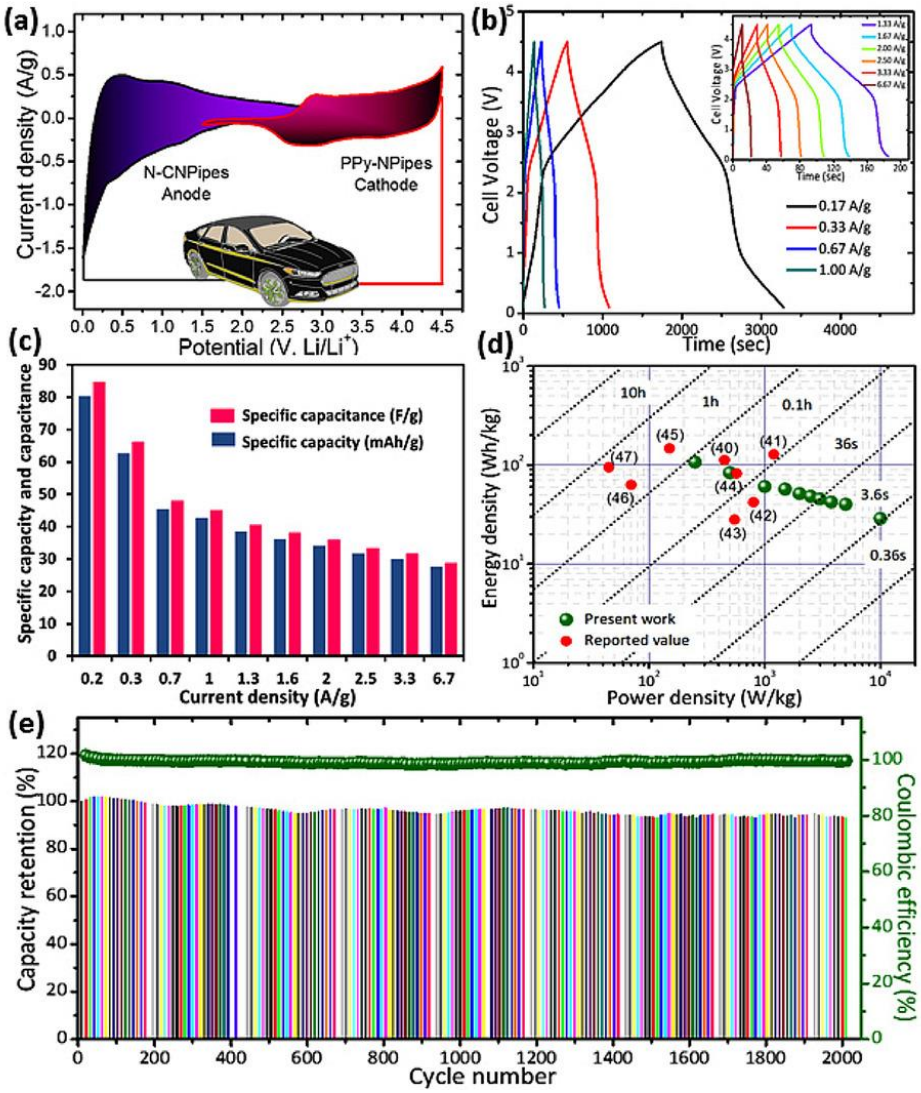

Figure 5 Electrochemical peformances of Full cell: (a) CV curves for both N‐CNPipes and PPy‐NPipes electrodes within potential windows of 0.01–3V and 1.5–4.5V (vs. Li/Li^+). (b) GCD curves for N‐CNPipes//PPy‐NPipes LIC at various current densities range from 0.17 to 6.67A/g. (c) Plot of specific capacity and capacitance versus the current density (d) Ragone plot with comparison with literature values. (e) Cycling stability with coulombic efficiency measured at current density of 1A/g over 2000 cycles.